

# Spectral line response to temperature perturbation in solar and stellar photospheric models

## I. Neutral Fe I line 522.5 nm case

J. Koza and A. Kučera

*Astronomical Institute of the Slovak Academy of Sciences  
059 60 Tatranská Lomnica, The Slovak Republic*

Received: March 13, 2002

**Abstract.** The sensitivity of the line profile of the neutral Fe I 522.5 nm line to Gaussian perturbations of temperature distribution in the photospheric models is examined. Stokes I response functions to temperature of the Fe I 522.5 nm line have been calculated using different classes of the solar photospheric models. In the LTE approximation three one-component models HOLMU, HSRA, VAL3C and a new two-component photospheric model are tested. In the  $(\log \tau_5, \lambda)$  plane the response functions have been calculated for all four models. It is shown that in the case of one-component models, the temperature perturbation in the upper photospheric layers only affects the core of the line profile and in contrast, the temperature perturbation of the deep photosphere affects only the line-wings. This is not the case in the two-component model, where the heating or cooling of the upper photosphere significantly modifies not only the line-core but also the wings. A detailed examination of this effect is presented and discussed to point out the incompatibility of simplified one-component models with the real physical conditions of the stellar photosphere.

**Key words:** solar photosphere – line formation – line profiles – perturbations

## 1. Introduction

The main task of the interpretation of spectra is the 'translation' of observational data into physical quantities commonly used for the description of the stellar atmosphere. If interpretation technique allows the vertical run of some physical quantities to be inferred from the spectrum, then the run represents the structure of the stellar atmosphere or some particular atmospheric phenomenon, which may be spatially resolved or unresolved in the spectrum.

The considerable effort to understand the solar atmosphere as a whole has culminated in a number of semiempirical models. Let us mention as representative examples the Harvard-Smithsonian Reference Atmosphere (HSRA),

(Gingerich et al., 1971); Holweger Müller Atmosphere (HOLMU), (Holweger & Müller, 1974) and the average quiet Sun model (VAL3C), (Vernazza et al., 1981). They can be considered as a certain class of the atmospheric models having the following characteristics:

- description of the photosphere and chromosphere (except HOLMU);
- one-component 1D models disregard granulation, thus unable to reproduce asymmetrical line profiles;
- predominately, the observational data were continuum intensities in the IR, visible and UV spectral ranges. Only a minority of the data covered the strongest spectral lines.;
- all atmospheric motions assigned as 'dynamics' are expressed with 'macro-' and 'microturbulence' without taking into account the actual granular flow of matter. (Although the VAL models describe different components of the solar atmosphere, they neglect granulation.);

A new superior inversion method joined the spectral diagnostic techniques in the last decade (Ruiz Cobo & del Toro Iniesta, 1992). The powerful capabilities of this approach especially applied on spectra with high spectral resolution allowed the formulation of a new atmospheric model class. To stress the differences between the two classes of models, some characteristics of the new one could be itemized:

- description is limited to just the photosphere;
- spatially resolved granulation (Rodríguez Hidalgo et al., 1995) and granulation manifested just through asymmetry of the spatially averaged profiles (Borrero & Bellot Rubio, 2002) is properly involved in two-component 1D models;
- used observational data is exclusively Fe I line profiles obtained from the solar disc center with high spectral resolution but with different spatial resolution;
- besides conventional micro- and macroturbulence, the flow of matter in granule and intergranule is characterized by line-of-sight velocity referred to as  $v_{\text{LOS}}$ ;

In the period of the 80's and 90's the principal questions regarding contribution and response functions (CFs, RFs) were clarified, because they are strongly related with the concept of the height of formation of spectral lines (see e.g. Caccin et al. (1977), Magain (1986), Sarychev (1986), Grossmann-Doerth et al. (1988), Gurtovenko et al. (1991), Ruiz Cobo et al. (1994), Sánchez Almeida et al. (1996) and references therein). In contrast, the CFs were investigated in Kučera et al. (1998) from an experimental point of view.

This paper aims to demonstrate, that a more realistic two-component model involving velocity gradients breaks down the symmetry of the Stokes I RFs for temperature with consequences in the shape of the line profile.

## 2. Theoretical outline

The CFs show explicitly the relevant layers of the atmosphere which contribute to a large extent to the observed intensity at a given wavelength, whereas the RFs inform us of the response of the observed spectrum to changes in the assumed atmospheric parameters (del Toro Iniesta, 2001). More exactly, RFs can be viewed as the partial derivatives of the spectrum with respect to the various parameters defining the model. Among all possible RFs with respect to atmospheric parameters the RF for temperature plays the paramount rôle, because its peak magnitudes are greater by about one or more orders than the peak magnitudes of RFs for other atmospheric parameters (e.g. Ruiz Cobo & del Toro Iniesta, 1992, 1994). That is the main reason why this paper deals with just RFs for temperature. The RFs for other atmospheric parameters will be the subject of examination in Paper IV of this series.

Both CFs and RFs are model dependent and vary strongly across the wavelength span of a given line. If CFs are calculated using any of idealized one-component models, their overall shapes support the conviction that line-wing photons on average come from deeper layers than line-core photons, as is readily seen from CFs shape (del Toro Iniesta, 2001). This statement could be reformulated for RFs to the form, that line-wing is more sensitive to perturbations in deeper layers, whereas line-core is more sensitive to variations in upper layers. To date, there are not objections bringing into question these statements.

## 3. Line selection and Fe I 522.5 nm line parameters

The complex atomic structure of iron ensures that in particular neutral Fe I and single ionized Fe II lines are highly abundant in the solar spectrum and differ regarding diagnostic capabilities. The appropriate thermodynamic state of atmospheric layers determines the occurrence of a specific bound-bound transition in the spectrum. Therefore Fe I and Fe II lines are often considered as sensitive probes of the atmosphere, i.e. they are assumed to provide information about many different so called line-forming layers depending on their atomic parameters. Hence, selection of a Fe I line constrains the range of relevant layers and inferences valid for strong Fe I lines can not be generalized for weak Fe I lines and vice versa. As we just deal with the representation of medium-strong Fe I lines in this paper, the representations of weak Fe I and ionized Fe II lines will be the subjects of examination in Paper II and Paper III of this series. Last but not least, the most important attribute for our calculations must be stated, that

LTE is a reasonable approximation for Fe I at least for 1D model atmospheres of solar-type stars (Shchukina & Trujillo Bueno, 2000).

Recently, a relatively unknown medium-strong Fe I 522.5 nm line appeared as a spectroscopic tool in a few studies (e.g. Kučera et al., 2000a, 2000b). The line is highly magnetic sensitive, because its Landé factor  $g_{\text{eff}}$  is 2.25 (Beckers, 1969). As input atomic parameters describing the transition considered the SIR code (see Chap.4.) needs following quantities: the central (air) laboratory wavelength of the transition, which is 522.55261 nm (Nave et al., 1994). the excitation potential of the lower level 0.11 eV, oscillator strength  $\log(gf) = -4.74$  and iron abundance 7.46 were taken from Thévenin (1989) and the enhancement factor of van der Waals broadening  $\Gamma_6$  was set to 1.

## 4. Calculations

For the purpose of this work, Stokes Inversion based on Response functions code (hereafter SIR) developed by Ruiz Cobo & del Toro Iniesta (1992) is used. Three models: HSRA, HOLMU and VAL3C are adopted as suitable representatives of all one-component models. Their two-component counterpart is represented by the Borrero & Bellot Rubio (2002) model, which embraces granular and intergranular components, hereafter referred to as GR and IG. As a depth scale, the logarithm of continuum optical depth  $\log \tau_5$  at 500 nm is used for all models.

Calculations were performed in two steps. First, the RFs and line profiles of Fe I 522.5 nm line were calculated for the four standard models. Then the temperature perturbations were introduced at high and low levels of the photosphere to examine the influence of such perturbations on the line profile. Several manipulations and simplifications were made concerning the temperature and velocity stratification before starting the final calculations.

### 4.1. Temperature stratification

LTE assumed in the SIR code imposes certain constrains regarding layers, which must be excluded from HSRA and VAL3C models. Namely, both involve chromospheric layers with a characteristic temperature minimum and a following temperature rise. However, a significant difference between them is, that in the case of the VAL3C model the temperature minimum is deeper, near  $\log \tau_5 = -3.5$ , whereas in the HSRA model this is located at  $\log \tau_5 = -4$ . Thus, the layers from  $\log \tau_5 = 0.9$  to  $\log \tau_5 = -3.5$  were cut from all the models mentioned to work with models on an identical optical depth scale, but without an unwanted temperature rise. Moreover, the lower boundary was given by the base of the most 'shallow' model, which is HOLMU. Such truncated models were interpolated with uniform sampling  $\Delta(\log \tau_5) = 0.1$ . Finally, in accordance with the classification of individual atmospheric layers given in Gingerich et al. (1971), all the adopted models involve layers from the top of the convective region to the upper part of the photosphere.

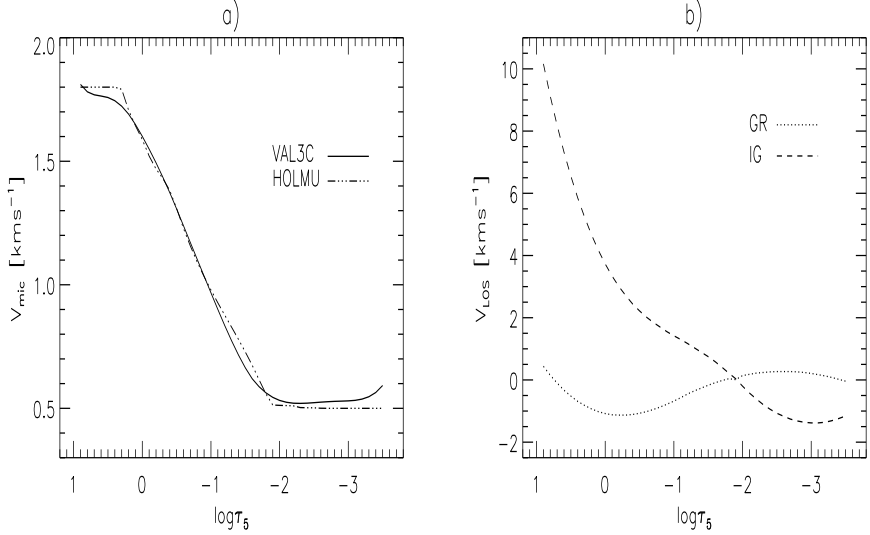


**Figure 1.** The stratification of the microturbulent velocity in VAL3C and HOLMU models (a). The stratification of the line-of-sight velocity representing flow of matter in the granular GR and intergranular IG parts of the two-component model Borrero & Bellot Rubio (2002). Positive velocities indicate downflows (b).

## 4.2. Velocity stratification

The macroturbulence is assumed to be height-independent in all models (see Tab. 1). The microturbulence for HSRA and two-component models are also constant throughout the atmosphere and the values of them are given in Tab. 1. The height-dependant microturbulences of HOLMU and VAL3C models are depicted in Fig. 1a). Because HSRA was inferred just from measurements of the continuum intensity, it does not primarily contain micro- and macroturbulence like other models, so they were fitted artificially by appropriate values, which do not affect the final results. Finally, the line-of-sight velocity  $v_{\text{LOS}}$  quantifying the matter flow inside granule and intergranule is shown in Fig. 1b) (Borrero & Bellot Rubio, 2002).

## 4.3. Filling factors

In adopted a two-component model the intensities emerging from each component,  $I_1$  and  $I_2$ , are computed individually and then mixed according to their filling factors  $f_1$  and  $f_2$  for granule and intergranule respectively. In this case, the emergent intensity  $I$  reads:

$$I = f_1 I_1 + f_2 I_2, \quad (1)$$

where  $f_1 = 0.76$  and  $f_2 = 0.24$ .

**Table 1.** Adopted macroturbulent and microturbulent velocities.

model	$v_{\text{mac}}$ [km s <sup>-1</sup> ]	$v_{\text{mic}}$ [km s <sup>-1</sup> ]
HSRA	1.0	0.6
HOLMU	1.6	—
VAL3C	0.4	—
GR	0.9	0.2
IG	1.0	2.0

#### 4.4. Code processing

In LTE the Stokes I response function to perturbation of temperature  $R_T$  is defined as:

$$R_T(\tau_5; \lambda) = \frac{e^{-\tau_\lambda}}{\alpha_5(\tau_5)} \left\{ \alpha_\lambda(\tau_5) \frac{\partial B_\lambda(\tau_5)}{\partial T} - \frac{\partial \alpha_\lambda(\tau_5)}{\partial T} [I_\lambda(\tau_5) - B_\lambda(\tau_5)] \right\}, \quad (2)$$

where  $\alpha_5(\tau_5)$ ,  $\alpha_\lambda(\tau_5)$  are the monochromatic extinction coefficients (unit m<sup>-1</sup>) at the optical depth  $\tau_5$  at 500 nm and a given wavelength  $\lambda$ ,  $B_\lambda(\tau_5)$  is the Planck function,  $I_\lambda(\tau_5)$  is the monochromatic intensity at the optical depth  $\tau_5$ ,  $\tau_\lambda$  is the optical depth at a given wavelength  $\lambda$  calculated by the formula:

$$\tau_\lambda = \int_0^{\tau_5} \frac{\alpha_\lambda}{\alpha_5} d\tau_5, \quad (3)$$

$e$  is the Euler number 2.71828... and  $T$  is temperature. A detailed derivation of the Eq. 2 in generalized vector form can be found in del Toro Iniesta (2001). A slightly modified form of Eq. 2 was also published in Caccin et al. (1977) under the reference (16) as a relative RF to temperature.

The calculations of synthetic line profiles and Stokes I RFs to temperature (Eq. 2) were performed by SIR code. In fact, the atmosphere is sampled in numerical calculations using a  $\log \tau_5$  scale instead of  $\tau_5$  and therefore SIR calculates  $R_T$  according to the formula:

$$R_T(x_i; \lambda) = R_T(\tau_{5i}; \lambda) \tau_{5i} \ln 10, \quad (4)$$

where  $x_i = \log \tau_{5i}$ . Index  $i = 1, \dots, n$  samples the individual layers of the atmosphere. Finally, the effect of the macroturbulence is simulated by convolving  $R_T(x_i; \lambda)$  and synthetic line profiles with a Gaussian:

$$M(\lambda - \lambda_0, v_{\text{mac}}) = \frac{1}{\sqrt{2\pi} \sigma} e^{-\frac{(\lambda - \lambda_0)^2}{2\sigma^2}}, \quad (5)$$

where  $\sigma \equiv \lambda_0 v_{\text{mac}}/c$ ,  $\lambda_0$  is the central wavelength of the transition,  $v_{\text{mac}}$  is the macroturbulent velocity and  $c$  is the speed of light (Bellot Rubio, 1999). For

completeness, the convolution may be written as:

$$R_{\text{T}}^*(x_i; \lambda) = M(\lambda) * R_{\text{T}}(x_i; \lambda). \quad (6)$$

The resulting  $R_{\text{T}}^*$  are absolute RFs in contrast to relative RFs (e.g. Ruiz Cobo & del Toro Iniesta, 1994). Thus they have unit  $\text{K}^{-1}$ . Both,  $R_{\text{T}}^*$  and synthetic profiles are normalized to the HSRA continuum intensity at the disk centre at the central wavelength of the Fe I 522.5 nm line, therefore the energetic unit is omitted.

As Eq. 2 and Eq. 4 indicate,  $R_{\text{T}}^*(x_i; \lambda)$  is a bivariate function of two independent variables: the logarithm of the optical depth  $x_i$  and the wavelength  $\lambda$ , which must be prescribed.  $R_{\text{T}}^*$  was calculated for optical depths running from  $\log \tau_5 = 0.9$  to  $\log \tau_5 = -3.5$ , which was reasoned in subsection 4.1. The  $R_{\text{T}}^*$  presented cover a wavelength span from  $-15$  pm to  $+15$  pm with respect to the central wavelength of the Fe I 522.5 nm line sampled with steps of 0.1 pm.

## 5. Results and discussion

### 5.1. Unperturbed atmospheres

Qualitative predictions are made in this subsection on the basis of the shapes of the  $R_{\text{T}}^*$ , whose correctness is verified on synthetic Fe I 522.5 nm line profiles in the next subsection.

The temperature stratifications of unperturbed one-component models are shown in Fig. 2a) and the  $R_{\text{T}}^*$  of the Fe I 522.5 nm line for unperturbed VAL3C, HSRA and HOLMU models are presented in Fig. 2b), c) and d) respectively. To gain a better insight into the information richness carried by  $R_{\text{T}}^*$ , their 3D graphical representations in the  $(\log \tau_5, \lambda)$  plane are given. At the first glance, some common features of the RFs are apparent:

- the  $R_{\text{T}}^*$  have global maxima in continuum forming layers and one local maximum near  $\log \tau_5 \simeq -3$ ;
- the  $R_{\text{T}}^*$  are symmetric with respect to line centre;
- the  $R_{\text{T}}^*$  for HOLMU is the most spread out because of the greatest macro-turbulence (see Tab. 1);

Consequently, the temperature perturbation located near  $\log \tau_5 \simeq 0$  (continuum forming layers) will affect just local continuum intensity and line-wings, whereas the line-centre will be untouched. On the contrary, the perturbations located somewhere between optical depths  $\log \tau_5 \simeq -2.5$  and  $\log \tau_5 \simeq -3.5$  affect just line-centre intensity. Moreover, the temperature change at any optical depth will affect the blue and red half of the line in the same way, i.e. the effect will be symmetrical.

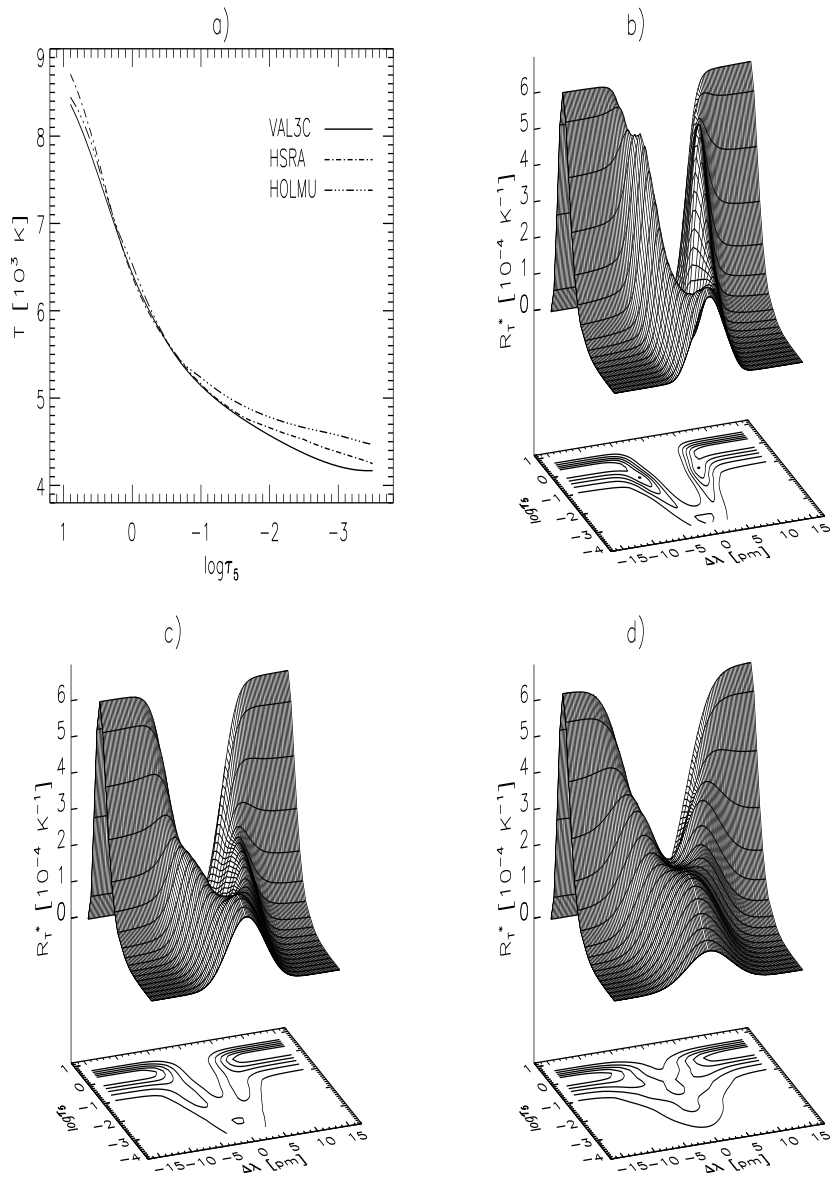


**Figure 2.** The temperature stratification of applied one-component models (a). Absolute Stokes I response functions to temperature  $R_T^*$  of the Fe I 522.5 nm line normalized to HSRA continuum at disk centre at the central wavelength of the line for VAL3C (b), HSRA (c) and HOLMU (d) model.

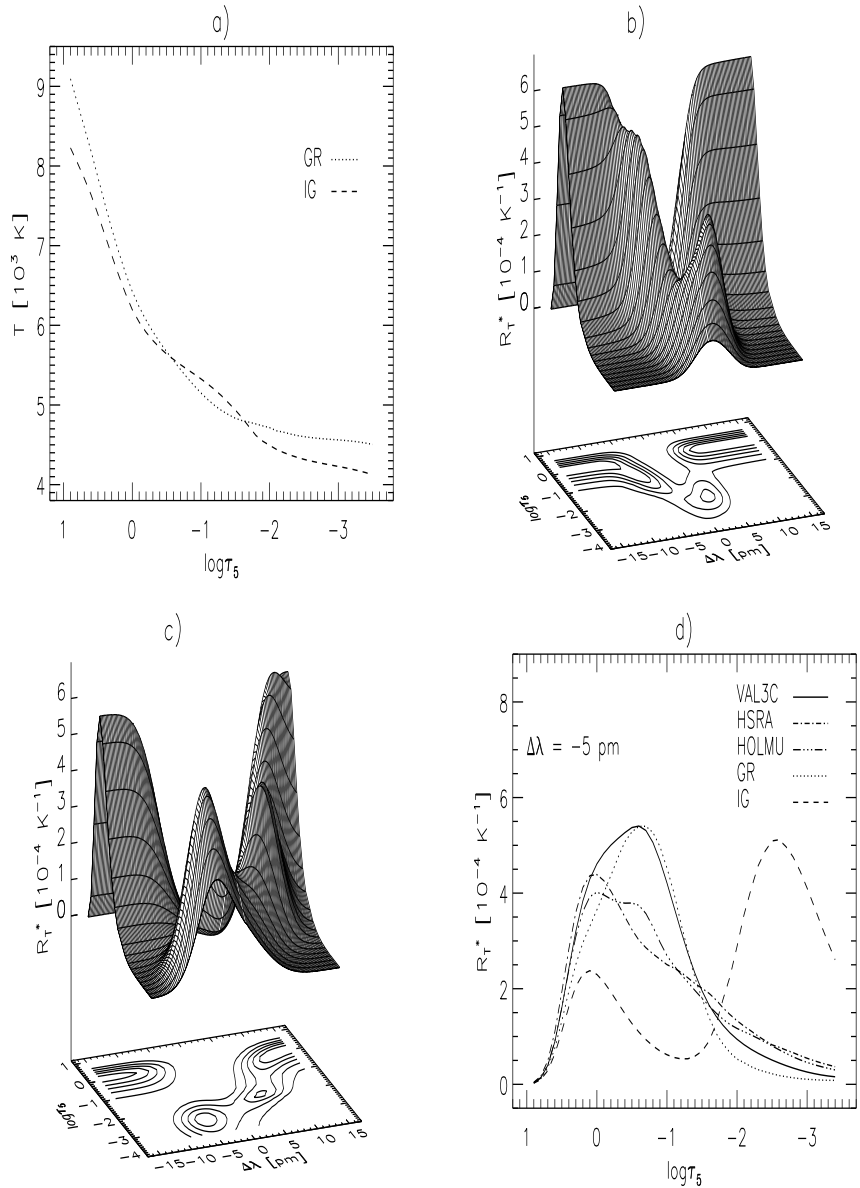


**Figure 3.** The temperature stratification for the two-component model Borrero & Bellot Rubio (2002) (a). Absolute Stokes I response functions to temperature  $R_T^*$  of the Fe I 522.5 nm line normalized to HSRA continuum at disk centre at the central wavelength of the line for the granular GR (b) and intergranular IG (c) parts of the two-component model. The cuts of  $R_T^*$  at  $\Delta \lambda = -5$  pm of the Fe I 522.5 nm line for indicated models (d).

Generally, using a more realistic two-component model, it was a challenge to verify traditional principles, which rest upon an idealized view of reality. In our case, this was done repeating the procedure outlined above, but using the Borrero & Bellot Rubio (2002) two-component model. In Fig. 3a) the temperature run of GR and IG atmosphere is shown together with the  $R_T^*$  for GR (Fig. 3b) and IG component (Fig. 3c) whose rugged shapes lead to the following conclusions:

- the  $R_T^*$  have global maxima in continuum forming layers similarly to one-component models;
- the  $R_T^*$  may possess more than one local maximum in upper layers, which are bigger and more pronounced than  $R_T^*$  for one-component models;
- the  $R_T^*$  are asymmetric with respect to line centre;

Hence, the temperature change will have a different influence on the blue and the red half of the line but the consequence of the temperature perturbation in continuum forming layers should be the same as in one-component models.

Whereas  $R_T^*$  for the GR component looks similar to  $R_T^*$  for one-component models (compare Fig. 3b) and Fig. 2b), c), d), the  $R_T^*$  for IG (Fig. 3c) is more striking with the double-peak in the upper layers. An isolated local maximum whose estimated central peak coordinates are  $\log \tau_5 \simeq -2.5$  and  $\Delta \lambda \simeq -5$  pm deserves a special attention. The extraordinary behaviour of the  $R_T^*$  for IG at this point is highlighted in Fig. 3d) more clearly. Because the point of line profile at  $\Delta \lambda = -5$  pm can be regarded as a part of the line-wing, it is possible to foresee on the base of Fig. 3b) and c), that the temperature perturbation around  $\log \tau_5 \simeq -2.5$  does not influence only the line-centre, but also the line-wing around  $\Delta \lambda \simeq -5$  pm, what is in contradiction to traditional understanding based on one-component models. It should be noted (see Fig. 2b), that the perturbation of e.g. VAL3C model in the same optical depth will produce a very small track on line-wing at  $\Delta \lambda = -5$  pm. A further logical step was to explicitly test the predictions given in this section.

## 5.2. Perturbed atmospheres

The wordy guesses made in subsection 5.1. are going to be demonstrated more clearly in this section. For this purpose, just the VAL3C model as a representative of the three one-component models is regarded along with its two modifications (see Fig. 4a), which differ to each other in optical depth, where the peak of Gaussian perturbation is located. The equations defining the first (dotted line in Fig. 4a) and the second (dashed line in Fig. 4a) modification have the form:

$$T_1(x) = T_0(x) + Ae^{-\frac{x^2}{B^2}}, \quad (7)$$

$$T_2(x) = T_0(x) + Ae^{-\frac{(2.5+x)^2}{B^2}}, \quad (8)$$

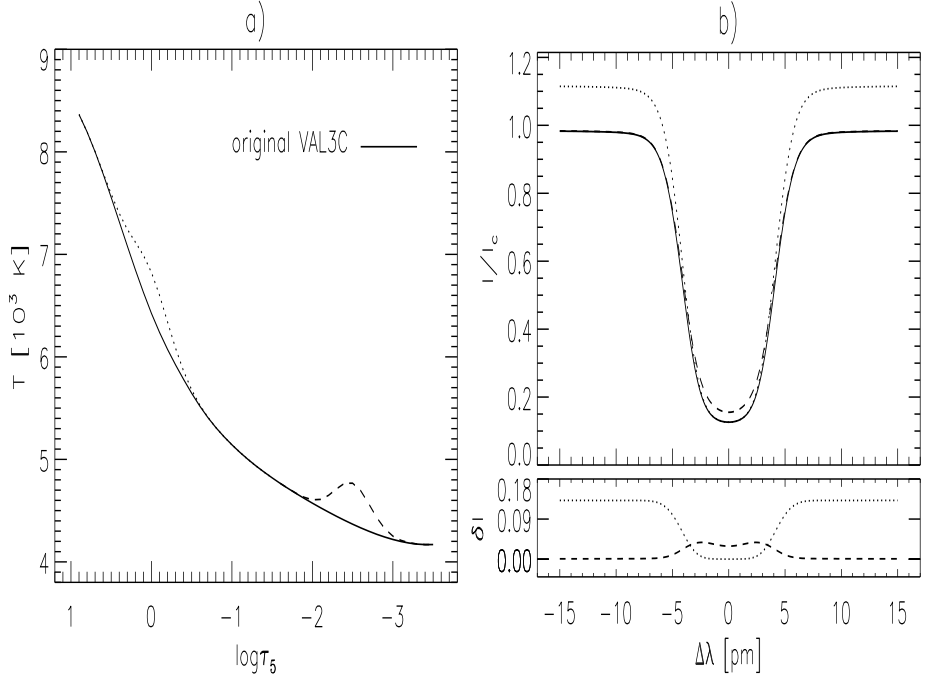


**Figure 4.** The temperature stratification of the VAL3C models, original VAL3C (solid), perturbed VAL3C in deeper layers around  $\log \tau_5 \simeq 0$  (dotted) and in upper layers around  $\log \tau_5 \simeq -2.5$  (dashed) (**a**). The synthetic Fe I 522.5 nm line profiles calculated by original VAL3C (solid, referred to as  $I_O$ ), perturbed VAL3C in deeper (dotted,  $I_D$ ) and upper (dashed,  $I_U$ ) layers (**b**, **upper panel**). The profiles are averaged in the sense of the spatial resolution.  $\delta I$  which correspond to  $I_D - I_O$  (dotted) and  $I_U - I_O$  (dashed) are shown at the bottom.

where  $T_0(x)$  is the original temperature run,  $x = \log \tau_5$ ,  $A = 400$  and  $B = 0.32$ . Thus,  $T_1(x)$  and  $T_2(x)$  represent the model perturbed in the continuum forming layers ( $\log \tau_5 \simeq 0$ ) and the upper layers ( $\log \tau_5 \simeq -2.5$ ) respectively. This set of three models (the original model and the two perturbed ones) was used in synthesis of the Fe I 522.5 nm line profiles shown in Fig. 4b). As can be seen, the behaviour of the profiles is consistent with the expectation derived from the overall shape of  $R_T^*$  in subsection 5.1, because continuum level and line-wings changed owing to the perturbation in deep layers, whereas the line-centre variation was induced by perturbation in the upper layers. We recall that synthetic profiles resulting from one-component models must always be regarded as average or spatially unresolved, which is a main sign of stellar spectra.

Similarly, to provide an explicit test of the predictions given for two-component models, two modifications of the IG model were created (see Fig. 5a) applying Gaussian perturbations (Eq. 7 and Eq. 8) on the original IG model.

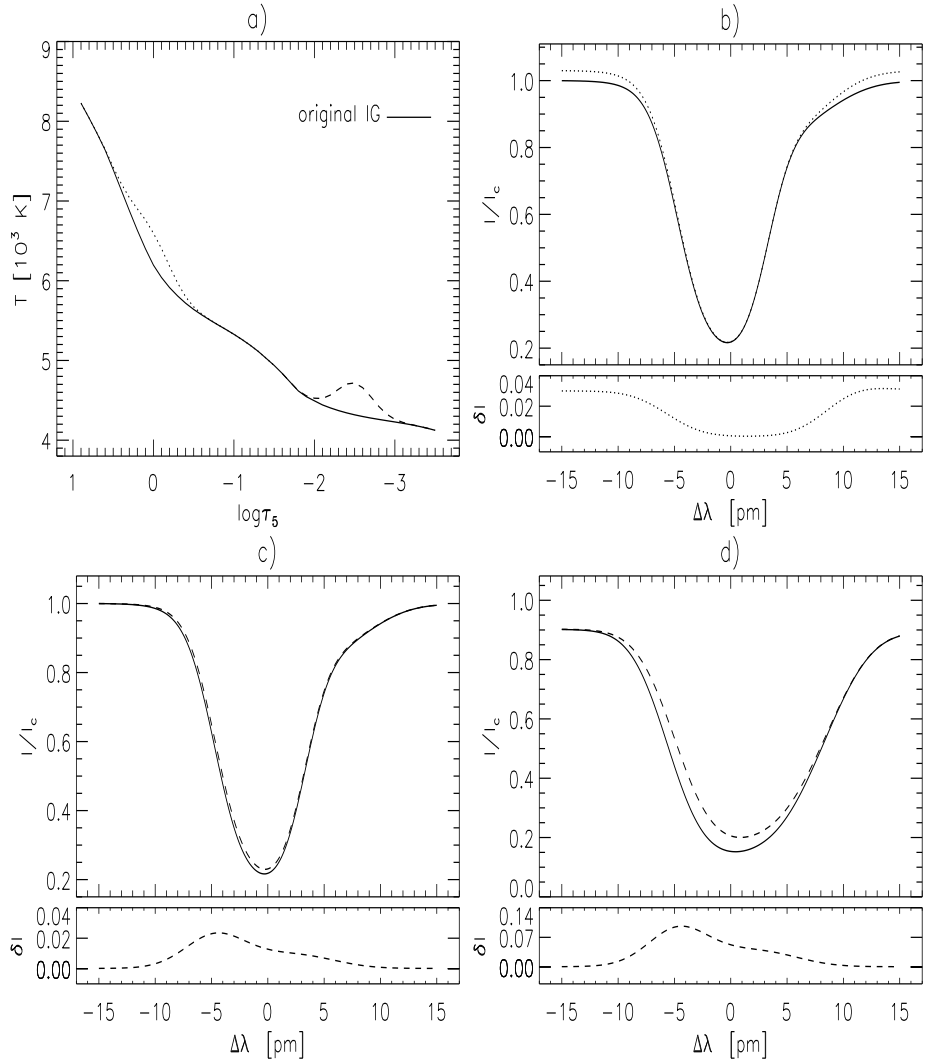


**Figure 5.** The temperature stratification of the IG component of the two-component model Borrero & Bellot Rubio (2002) (a), IG perturbed in deeper layers around  $\log \tau_5 \simeq 0$  (dotted) and in upper layers around  $\log \tau_5 \simeq -2.5$  (dashed). The synthetic Fe I 522.5 nm line profiles calculated by the original IG model (solid, referred to as  $I_O$ ), perturbed in deeper (dotted,  $I_D$ ) and upper (dashed,  $I_U$ ) layers (b, c, d, **top panel**).  $\delta I$  which correspond to  $I_D - I_O$  (dotted) and  $I_U - I_O$  (dashed) are shown at the bottom. The profiles may be regarded as a simulation of spatially unresolved intergranular profiles (b), (c) and spatially resolved profiles (d). The unperturbed GR component was entered into the calculation of spatially unresolved profiles via Eq. 1.

Intentionally, the GR model will enter unchanged into the line synthesis, because of its greater filling factor and the similarity already mentioned between its  $R_{\text{T}}^*$  and  $R_{\text{T}}^*$  for one-component models. Therefore introducing the same perturbation into the GR model could not yield anything new and should result in the same conclusion as in the case of a perturbed one-component model. In fact, we want to unmask the influence of perturbation in a model with the most unusual  $R_{\text{T}}^*$  on spatially unresolved profiles. Such profiles are characteristic for all stellar spectra.

The spatially unresolved synthetic profiles resulting from the original two-component model and the two-component model with a perturbed IG component are shown in Fig. 5b) and c). The contribution of the GR and IG model to the resulting profile is mixed by filling factors (see Eq. 1). Therefore the amplitude of variations is reduced in comparison with previous cases. Fig. 5b) and c) say, in accordance with expectation, that continuum level and line-wings react to the perturbations in the continuum forming layers, however simulated perturbation of upper layers leads to considerable line-wing variation as well but with an asymmetric effect, just at point  $\Delta\lambda = -5$  pm.

The spatially resolved synthetic intergranular profiles resulting just from unperturbed and in upper layers perturbed IG component are shown in Fig. 5d). Because the Sun is the only astrophysical object where it is possible to observe spatially resolved granular and intergranular profiles, the shown profiles might exemplify the impact of such perturbations on real spectra.

It is worth pointing out, that profiles obtained from the two-component model are evidently asymmetric with slightly blue-shifted line-centre, which is in contrast with symmetric and with respect to laboratory wavelength non-shifted profiles resulting from one-component models. Undoubtedly, the two-component model gives a more realistic description of the stellar photosphere. Other shape dissimilarities of the compared profile can be explained by the inherent properties of the VAL3C, GR and IG model, but that is not the subject of our interest.

### 5.3. Is the point at $\Delta\lambda = -5$ pm part of the line-wing ?

A final remark should be devoted to the issue of whether the line profile point at  $\Delta\lambda = \mp 5$  pm may be regarded as a part of the line-wing or not. The first-order simplification of the problem is an approximation of the Fe I 522.5 nm line profile with a pure Doppler profile. Then the Doppler width  $\Delta\lambda_{\text{D}}$  is the most natural way to define the line-core and the line-wing. Those profile points for which  $\Delta\lambda \leq \Delta\lambda_{\text{D}}$ , may be regarded as parts of line-core, whereas the points for which  $\Delta\lambda > \Delta\lambda_{\text{D}}$ , are parts of the line-wing. The Doppler width of the line is given by the well-known formula:

$$\Delta\lambda_{\text{D}} = \frac{\Delta\lambda}{c} \sqrt{\frac{2kT}{m} + v_{\text{mic}}^2}, \quad (9)$$

where the symbols used have usual meaning (see e.g. Gray, 1976). Applying Eq. 9 we found out that  $\Delta\lambda_D$  for FeI 522.5 nm line is smaller than 5 pm for all layers of the VAL3C, GR and IG model. The  $\Delta\lambda_D$  reaches a maximum value of 4.5 pm for the deepest layer at  $\log \tau_5 = 0.9$  of the IG model. Hence, it is justified to consider the profile point at  $\Delta\lambda = -5$  pm as a part of the line-wing.

## 6. Conclusion

The method presented in this paper suggests how to assess the impact of atmospheric perturbation on the line profile examining the RFs. Nevertheless, the information provided by the RFs is only qualitative in so far as they are model dependent. This characteristics of the RFs is readily seen, when the RFs are calculated for two-component model. Because  $v_{LOS}$  enters into RFs calculation (del Toro Iniesta, 2001), the RFs become more complicated with shifted and split maxima of sensitivity. In the particular case of the IG model, the resulting asymmetry and split is so strong that line-wing variation can not be ascribed to the changes of temperature structure of the deep layers only. Generally, the presence of velocity gradients associated with granulation in stellar atmospheres may considerably complicate the relationship between perturbed layer and line profile variation, if we think in terms of sharply localized perturbations. Although the output spectra presented do not show the flux but intensity, the general inference is valid for all stellar atmospheres suspected of granulation.

**Acknowledgements.** The authors are extremely thankful to Dr.J.Rybák for support with an IDL routine and Dr.J.Budaj for stimulating discussions as well as to P.Bendik for transcription of the tabulated models to electronic form. The work was partly supported by VEGA grant 7229.

## References

- Beckers, J.M.: 1969, *A Table of Zeeman Multiplets*, Air Force Cambridge Research Laboratories, Bedford, Massachusetts
- Bellot Rubio, L.R., 1999, *A user guide to SIR, Version 2*, manual
- Borrero, J.M., Bellot Rubio, L.R.: 2002, *Astron. Astrophys.* **385**, 1056
- Caccin, B., Gomez, M.T., Marmolino, C., Severino, G.: 1977, *Astron. Astrophys.* **54**, 227
- Gingerich, O., Noyes, R.W., Kalkofen, W., Cuny, Y.: 1971, *Sol. Phys.* **18**, 347
- Gray, D.F.: 1976, *The Observation and Analysis of Stellar Photospheres*, Wiley, New York
- Grossmann-Doerth, U., Larsson, B., Solanki, S.K.: 1988, *Astron. Astrophys.* **204**, 266
- Gurtovenko, E.A., Sheminova, V.A., Sarychev, A.P.: 1991, *Sol. Phys.* **136**, 239
- Holweger, H., Müller, E.A.: 1974, *Sol. Phys.* **39**, 19
- Kučera, A., Balthasar, H., Rybák, J., Wöhl, H.: 1998, *Astron. Astrophys.* **332**, 1069
- Kučera, A., Brčková, K., Hanslmeier, A., Rybák, J., Wöhl, H., 2000a, *Hvar Obs. Bull.*, **24**, 111

- Kučera, A., Brčková, K., Hanslmeier, A., Rybák, J., Wöhl, H., 2000b, in *1<sup>st</sup> Solar & Space Weather Euroconference, 'The Solar Cycle and Terrestrial Climate'*, ESA SP-463, 357
- Magain, P.: 1986, *Astron. Astrophys.* **163**, 135
- Nave, G., Johansson, S., Learner, R.C.M., Thorne, A.P., Brault, J.W.: 1994, *Astrophys. J., Suppl. Ser.* **94**, 221
- Rodríguez Hidalgo, I., Ruiz Cobo, B., del Toro Iniesta, J.C., Collados, M., Sánchez Almeida, J.: 1995, *JOSO Annual Report*, 162
- Ruiz Cobo, B., del Toro Iniesta, J.C.: 1992, *Astrophys. J.* **398**, 375
- Ruiz Cobo, B., del Toro Iniesta, J.C.: 1994, *Astron. Astrophys.* **283**, 129
- Sarychev, A.P.: 1986, *Astron. Zh.* **63**, 556
- Sánchez Almeida, J., Ruiz Cobo, B., del Toro Iniesta, J.C.: 1996, *Astron. Astrophys.* **314**, 295
- Shchukina, N., Trujillo Bueno, J.: 2000, in *Cool stars, stellar systems and the Sun*, 11th Cambridge workshop, in press
- Thévenin, F.: 1989, *Astron. Astrophys., Suppl. Ser.* **77**, 137
- del Toro Iniesta, J.: 2001, in *The Dynamic Sun*, eds.: Hanslmeier, A., Messerotti, M. and Veronig, A., Kluwer Academic Publishers, Dordrecht, 183
- Vernazza, J.E., Avrett, E.H., Loeser, R.: 1981, *Astrophys. J., Suppl. Ser.* **45**, 635